

doi:10.15199/48.2023.02.31

Scattering problems in 2D space within the Rayleigh regime

Abstract. In this paper, the application of the classic method of boundary elements to analyse the scattering problems of acoustic waves by a rigid object with a circular cross-section in 2D space is presented. The analysis is presented on the example of a flat wave falling on an object along the x -axis positive direction. The accuracy of the solution for two different cases meeting the Rayleigh regime was analysed. The criteria that must be met in order to expect a reliable solution are provided.

Streszczenie. W pracy przedstawiono zastosowanie klasycznej metody elementów brzegowych do analizy problemów rozpraszania fal akustycznych przez sztywny obiekt o przekroju kołowym w przestrzeni 2D. Analizę przedstawiono na przykładzie fali płaskiej padającej na obiekt zgodny z dodatnim kierunkiem osi x . Przeanalizowano dokładność rozwiązania dla dwóch różnych przypadków spełniających wymagania reżimu Rayleigh'a. Podano kryteria jakie muszą być spełnione, aby można było oczekiwać wiarygodnego rozwiązania (**Problemy rozpraszania w przestrzeni 2D w reżimie Rayleigha**).

Keywords: boundary element method, acoustics, Helmholtz equation, Rayleigh regime.

Słowa kluczowe: metoda elementów brzegowych, akustyka, równanie Helmholtza, reżim Rayleigh'a.

Introduction

Many numerical methods can be used to analyze forward, and inverse problems, are ultrasound tomography [1-14]. Considering acoustic scattering problems in infinite domains, BEM has become the preferable approach. The biggest advantage is that the Sommerfeld radiation condition [15] is satisfied by an open boundary problem (Fig. 1). Thus, there is no requirement to truncate the domain and impose artificial non-reflecting boundary conditions.

The problem is outlined by beginning with the time-harmonic reduction of the wave equation for the exterior problem to the Helmholtz equation and finally to the Boundary Integral Equation formulation [16] for the acoustic scattering problem. The sound-hard scatterer is imposed through a homogeneous Neumann boundary condition on the boundary Γ (see Fig. 2). Making use of Green's second identity, the Helmholtz equation can be expressed in an equivalent form of a Boundary Integral Equation (BIE) [4], i.e.

$$(1) \quad c(\mathbf{r})\varphi(\mathbf{r}) + \int_{\Gamma} \frac{\partial G(|\mathbf{r}-\mathbf{r}'|)}{\partial n} \varphi(\mathbf{r}') d\Gamma = \int_{\Gamma} G(|\mathbf{r}-\mathbf{r}'|) \frac{\partial \varphi(\mathbf{r}')}{\partial n} d\Gamma + \varphi^{inc}(\mathbf{r}), \quad \mathbf{r} \in \Gamma$$

where φ^{inc} is the incident wave, and the vector \mathbf{n} is the unit normal vector outward pointing from the considered domain, see the centre of figure 1.

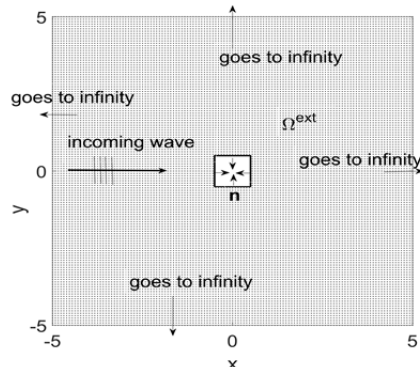


Fig. 1. Internal point locations for an arbitrary shape scatterer (in this figure, square one)

Due to the homogeneous Neumann boundary conditions, the third term of Eq. (1) vanish. Now the integral

boundary equation (1) for constant boundary elements can be written in terms of local coordinate ξ as follows:

$$(2) \quad c(\mathbf{r})\varphi(\mathbf{r}) + \sum_{j=1}^M \varphi_j(\mathbf{r}') \int_{-1}^{+1} \frac{\partial G(|\mathbf{r}-\mathbf{r}'|)}{\partial n} J(\xi) d\xi = \varphi^{inc}(\mathbf{r})$$

where M – is the total number of constant elements and $J(\xi)$ – is the Jacobian of transformation, which for constant element is equal to:

$$(3) \quad J(\xi) = \frac{d\Gamma}{d\xi} = \sqrt{\left(\frac{dx(\xi)}{d\xi}\right)^2 + \left(\frac{dy(\xi)}{d\xi}\right)^2} = \frac{L}{2}$$

where L is the length of the constant boundary element [16].

If the plane wave is travelling along the vector $\mathbf{d}_j = (\cos \theta_j, \sin \theta_j)$ then $\varphi^{inc}(\mathbf{r}) = e^{i\mathbf{k}\mathbf{r}\cdot\mathbf{d}_j}$, where i is the imaginary unit $i = \sqrt{-1}$.

It is worth noticing that the unit vector is defined in the boundary element method by the x -component and y -component of the vector. So, the incoming wave is relatively easy to calculate on the boundary and incorporate into the right-hand side of the equation (2).

Plane-wave and circular scatterer for Neuman (hard wall) boundary conditions

In this chapter, we consider the scattering within the Rayleigh regime. By the Rayleigh regime [3] we understand the situation when the wavelength of scattering waves is much bigger than the diameter of the circular scatterer.

The simulation of the scattering problems is an extremely difficult task. The most important is controlling the correctness and precision of the solution. There are several different methods to control solutions.

The best method is to compare the results of numerical simulation with the analytical solution. Unfortunately, only the geometrically simplest scatterers are able to provide analytical solutions. The analytical solutions exist only for a narrow number of scatterers in the shape of a circle for 2D space and in the shape of a ball for 3D space.

In this chapter, we will restrict scatterers to the shape of circles only. Although the transition from circle to square looks like an easy step forward but additional serious problems associated with square scatterers will not be of interest to us in this paper.

Another method of validating the BEM simulation results is to compare them with the results presented in the literature or compare them with a solution obtained by another method, such as FEM or FDM (Finite Difference Method).

Moreover, finally, the most desirable but difficult and sometimes even impossible to implement there is a method of comparing the results of numerical simulation with measurement results.

Otherwise, in order for the results would be reliable, one can use tips taken from the literature. And here are the most important of them:

- 1) The number of boundary elements should be no less than 6 to 10 per wavelength (see, for example, [8]).
- 2) It is well known in the literature that BEM provides unreliable results for all but low wavenumber [7]. The wavenumber should fulfil the following relation:

$$kD < 4.0,$$

where D denote the diameter of the circular body and when the shape of the body is irregular then the maximum distance between two boundary points. But in [7] the author state that this condition is too restrictive for most of the applications, and as we can see later, this condition alone do not guarantee high precision of the solution.

In this paper, to control the simulation results, we will compare them with the analytical solution which was presented in [9]. Let the rigid circular void would be illuminated by the plane wave. The void is located in the centre of the cartesian system of coordinates, as it is shown in Fig. 2. The environment is the air with well-known parameters (see for example [8]).

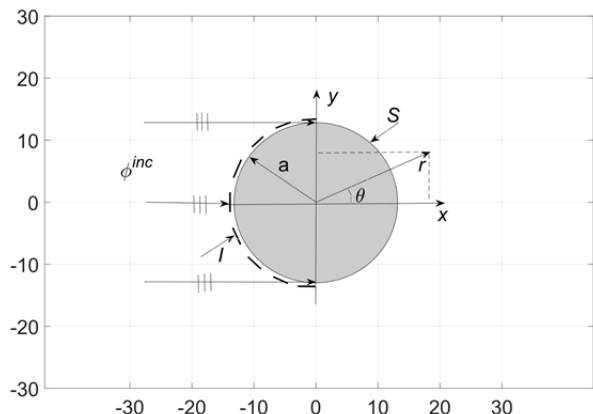


Fig. 2. Circular scatterer illuminated by a plane wave where I denote the illuminated and S denotes shadow zone

Let us consider a circular scatterer of radius $r = a = 1$, in the case of an incoming plane wave with incident angle θ , as shown in Fig. 2. Potential of the time-harmonic incoming wave can be expressed as [9]:

$$(4) \quad \varphi^{inc}(x, y) = e^{-ikr} = e^{-ik(x\cos\theta + y\sin\theta)}.$$

Our goal is to find out the total velocity potential composed of the incident and scattered velocity potential:

$$(5) \quad \varphi(x, y) = \varphi^{inc}(x, y) + \varphi^{scat}(x, y).$$

Velocity potential described by Eq. (5) satisfies the Helmholtz equation in integral form (see Eq. (2)). Due to the shape of the scatterer, it is convenient to introduce the polar coordinate system with origin in the centre of the circular scatterer:

$$(6) \quad x = r \cos\theta, \quad y = r \sin\theta.$$

We will be looking for the solution using the separation of variables method in the shape of [19]:

$$(7) \quad \varphi_n(r, \theta) = \left(A_n H_n^{(1)}(kr) + B_n H_n^{(2)}(kr) \right) e^{in\theta},$$

where $H_n^{(1)}(kr)$ and $H_n^{(2)}(kr)$ are the Henkel functions of the first and second kind respectively [1].

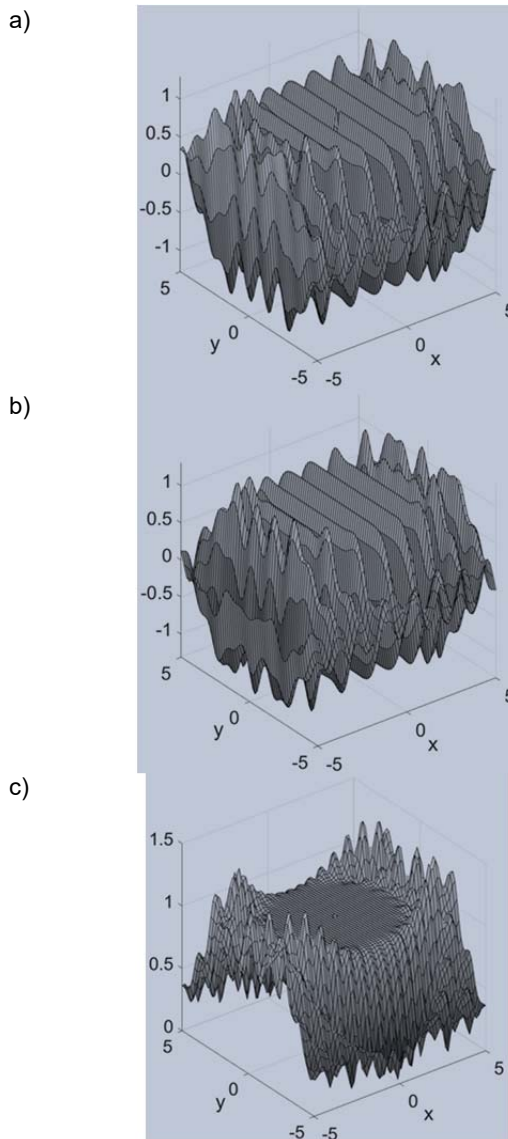


Fig. 3. Incoming flat wave with unit amplitude expansion for only 20 modes a) real part b) imaginary part and c) the absolute value.

As the region extends to infinity, only the outgoing wave will be taken into consideration, it means that the scattered field can be a sum of the modes $\varphi_n(r, \theta)$:

$$(8) \quad \varphi^{scat}(r, \theta) = \sum_{n=-\infty}^{\infty} i^n A_n H_n^{(1)}(kr) e^{in(\theta - \theta_0)},$$

or:
(9)

$$\varphi^{scat}(r, \theta) = A_0 H_0^{(1)}(kr) + 2 \sum_{n=1}^{\infty} i^n A_n H_n^{(1)}(kr) \cos(n(\theta - \theta_0)),$$

where A_n is the amplitude of the n -th mode.

To determine the amplitudes A_n we have to use the homogeneous Neumann boundary conditions:

$$(10) \quad \frac{\partial \varphi}{\partial r} = 0 \quad \text{on } r = a.$$

Following Eq. (5), the incident plane wave with unit amplitude will express as an infinite sum of the first kind of Bessel functions using the Jacobi-Anger expansion [1]. It is shown in the figures below

The plane wave is travelling from the left in the positive direction of the x-axis direction toward a cylindrical gap with a rigid boundary. Fig. 3 shows a plot for only 20 terms of cylindrical Bessel functions. In Fig., it can clearly see the influence of the limited number modes in the shape of a circular pattern.

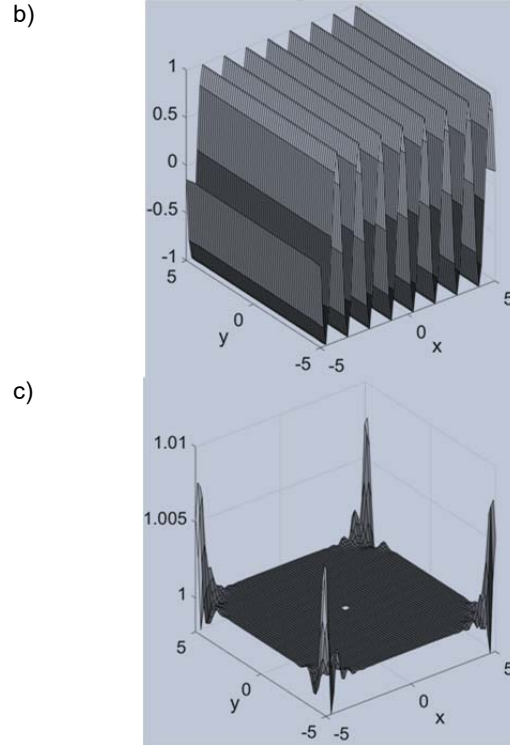
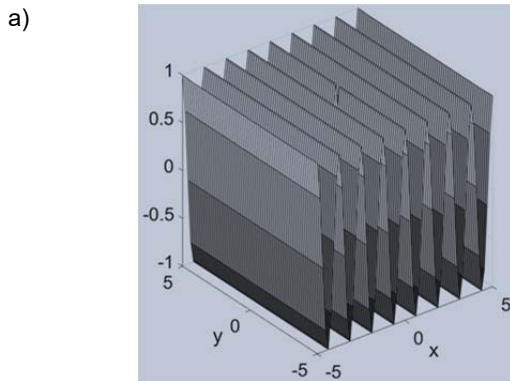


Fig. 4. Incoming flat wave expansion for 40 modes a) real part b) imaginary part and c) the absolute value for unite amplitude

are some perturbances with an error less than 1%.

The higher frequency of the wave the more terms of the flat wave expansion has to be selected.

$$(11) \quad \varphi^{inc}(r, \theta) = e^{i kr \cos(\theta - \theta_0)} = \sum_{n=-\infty}^{\infty} i^n J_n(kr) e^{i n(\theta - \theta_0)},$$

where θ is the polar coordinate and θ_0 is the angle of incoming plane wave.

Using the relation $J_{-n}(kr) = (-1)^n J_n(kr)$ the incoming wave could be expressed as follows [2]:

$$(12) \quad \varphi^{inc}(r, \theta) = e^{i kr \cos(\theta - \theta_0)} = J_0(kr) + 2 \sum_{n=1}^{\infty} i^n J_n(kr) \cos(n(\theta - \theta_0)).$$

Following Eq. (5) we have got the complete solution: (13)

$$\varphi = J_0(kr) + A_0 H_0^{(1)}(kr) + 2 \sum_{n=1}^{\infty} i^n \left(J_n(kr) + A_n H_n^{(1)}(kr) \right) \cos(n(\theta - \theta_0)).$$

Each term of the expansion (13) is called a partial wave [2]. Now for the Neumann boundary conditions, it can calculate the amplitudes of n -th mode of the wave as:

$$(14) \quad A_n = - \frac{J_n'(ka)}{H_n^{(1)'}(ka)}$$

where the prime sign denotes derivatives with respect to the argument ka and a is a radius of the circular void (see Fig. 2).

However, by increasing the number of terms up to 40 we can easily notice the flat wave pattern (see Fig. 4c). Only at the corners of an image there

Following the works [1,3] we will have:

$$(15) \quad J_0'(ka) = -J_1(ka)$$

$$(16) \quad J_n'(ka) = \frac{1}{2} (J_{n-1}(ka) - J_{n+1}(ka)),$$

and similarly for Hankel functions, we have got:

$$(17) \quad H_0^{(1)'}(ka) = -H_1^{(1)}(ka)$$

$$(18) \quad H_n^{(1)'}(ka) = \frac{1}{2} (H_{n-1}^{(1)}(ka) - H_{n+1}^{(1)}(ka))$$

Then the amplitude of the n -th mode will be:

$$(19) \quad A_0 = - \frac{J_0'(ka)}{H_0^{(1)'}(ka)} = - \frac{-J_1(ka)}{-H_1^{(1)}(ka)}$$

$$(20) \quad A_n = - \frac{J_n'(ka)}{H_n^{(1)'}(ka)} = - \frac{J_{n-1}(ka) - J_{n+1}(ka)}{H_{n-1}^{(1)}(ka) - H_{n+1}^{(1)}(ka)}.$$

According to Eq. (5) the sum of incident and scattered wave will take the form:

$$(20) \quad \varphi(r, \theta) = J_0(kr) + A_0 H_0^{(1)}(kr) + 2 \sum_{n=1}^{\infty} i^n \left[J_n(kr) + A_n H_n^{(1)}(kr) \right] \cos(n(\theta - \theta_0))$$

Of practical interest is the potential angular distribution on the rigid boundary of the cylindrical void for $r = a$ namely $\varphi(a, \theta)$.

Numerical simulation

Let's consider two cases that meet Rayleigh's regime. In both cases, the wavelength is much larger than the diameter of the object, which fulfil Rayleigh regime conditions.

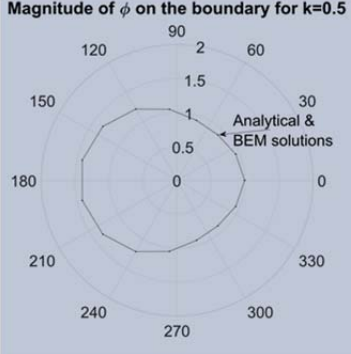
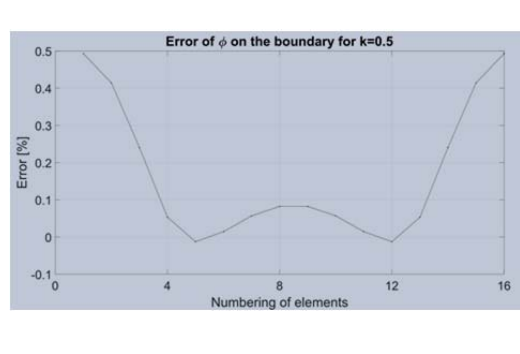
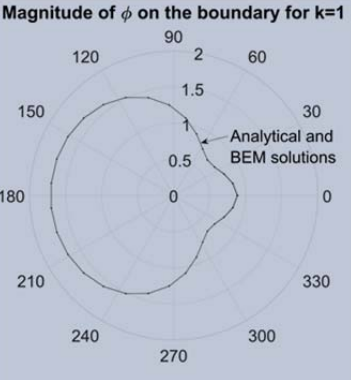
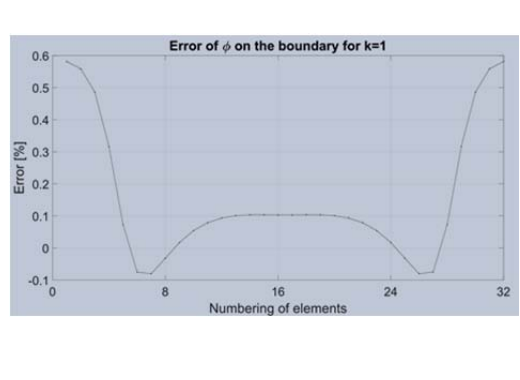
Comparison BEM and analytical magnitude on the boundary of the object	Error distribution along the perimetry of the scatterer	Basic data
<p>Magnitude of ϕ on the boundary for $k=0.5$</p> 	<p>Error of ϕ on the boundary for $k=0.5$</p> 	<p>wavelength $\lambda = 12.6\text{ m}$ frequency= 27.37 Hz boundary element length $L = 0.392\text{ m}$ number of boundary elements per wavelength $ne_per_lambda = 32$ $kD = 1 < 4.0$</p>
<p>Magnitude of ϕ on the boundary for $k=1$</p> 	<p>Error of ϕ on the boundary for $k=1$</p> 	<p>wavelength $\lambda=6.3\text{ m}$ frequency= 54.75 Hz boundary element length $L = 0.196\text{ m}$ number of boundary elements per wavelength $ne_per_lambda = 32$ $kD = 2 < 4.0$</p>

Fig. 5. Magnitude of the incoming and scattered wave on the perimetry of the circular void (scatterer); in the middle column the error distribution along the object boundary; and in the third column the basic data of the simulation

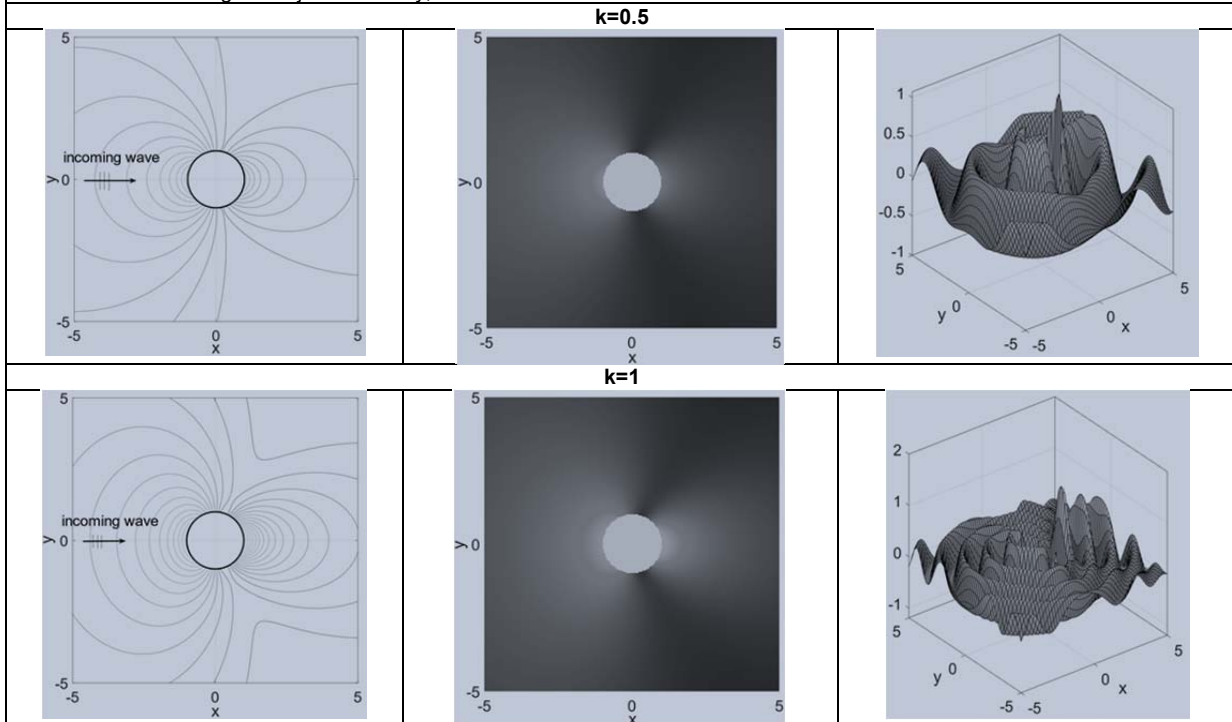


Fig. 6. Equipotential lines (left column), image of the potential velocity of sound with the sound shielding effect (middle column) and the relief image of the problem (right column)

In the first column figure, 5 shows a comparison of BEM results with an analytical solution. The level of the error is so low that both curves are almost the same. In the second column the distribution of the relative error along the edge of the area, while in the third column the basic parameters of the experiment. The air was an environment in this experiment.

The analytical solution was treated as a reference result. We must remember that the analytical solution is an infinite series truncated to 20 or 40 components. So, this is not an accurate result.

In the middle column relative error of the velocity potential magnitude along the rigid surface of the circular

scatterer is below one per cent. Such precision was achieved in spite of as coarse discretization as possible.

In Fig. 6, the first column (left) presents the equipotential lines of velocity potential, the next image of the potential velocity of sound with the sound shielding effect (middle column) and the third column relief image of the problem (right column). All results are presented for two cases where arguments of the Bessel functions are the small ones.

It should be emphasized that the calculation was carried out for the standard BEM. Accuracy improvement, particularly for higher frequencies, by simply increasing discretization does not give satisfactory results due to tomography applications. For the iterative mode of the tomography, we need as small number of unknowns as possible. According to the authors, the only solution seems to be the application of more sophisticated approximation like plane wave basis functions for example.

Conclusion

The acoustic scattering problem in 2D space was presented in this paper. The classical BEM was used, and its precision was analysed using the analytical solution as the reference one. Illuminated and the shadowed side of the circular scatterer were presented in the figures. The relative error distribution along the perimetry of the scatterer was calculated. The main goal of this paper was to investigate such an approach to tomography problems in acoustic or even ultrasonic problems. The errors were on the acceptable level, but more sophisticated basis functions could be necessary for high-frequency scattering problems in the future.

Authors: *prof. dr hab. inż. Jan Sikora^{1,2}, e-mail: sik59@wp.pl*, 1) *Research & Development Centre Netrix S.A., Związkowa 26, 20-148 Lublin, Poland;* 2) *University of Economics and Innovation in Lublin, ul. Projektowa 4, 20-209 Lublin, Poland;*

REFERENCES

- [1] Abramowitz M., Stegun I.A., Handbook of mathematical functions with formulas, graphs and mathematical tables. John Wiley, New York, (1973).
- [2] Akylas T.R., Mei C.C., I-campus project School-wide Program on Fluid Mechanics Modules on Waves in fluids. Chapter Five of Reflection, Transmission and Diffraction. <http://web.mit.edu/fluids-modules/waves/www/c-index.html>
- [3] Baynes A.B., Scattering of low-frequency sound by compact objects in underwater waveguides, Naval Postgraduate School, Monterey, California, PhD Dissertation, 2018.
- [4] Becker A.A., The boundary Element Method in Engineering. A complete course. McGraw-Hill Book Company, 1992.
- [5] Rymarczyk T., Kłosowski G., Hoła A., Sikora J., Tchórzewski P., Skowron Ł., Optimising the Use of Machine Learning Algorithms in Electrical Tomography of Building Walls: Pixel Oriented Ensemble Approach, Measurement, 188 (2022), 110581.
- [6] Koulountzios P., Rymarczyk T., Soleimani M., Ultrasonic Time-of-Flight Computed Tomography for Investigation of Batch Crystallisation Processes, Sensors, 21 (2021), No. 2, 639.
- [7] Kłosowski G., Rymarczyk T., Niderla K., Rzemieniak M., Dmowski A., Maj M., Comparison of Machine Learning Methods for Image Reconstruction Using the LSTM Classifier in Industrial Electrical Tomography, Energies 2021, 14 (2021), No. 21, 7269.
- [8] Rymarczyk T., Król K., Kozłowski E., Wołowicz T., Cholewa-Wiktor M., Bednarczuk P., Application of Electrical Tomography Imaging Using Machine Learning Methods for the Monitoring of Flood Embankments Leaks, Energies, 14 (2021), No. 23, 8081.
- [9] Majerek D., Rymarczyk T., Wójcik D., Kozłowski E., Rzemieniak M., Gudowski J., Gauda K., Machine Learning and Deterministic Approach to the Reflective Ultrasound Tomography, Energies, 14 (2021), No. 22, 7549.
- [10] Kłosowski G., Rymarczyk T., Kania K., Świć A., Cieplak T., Maintenance of industrial reactors supported by deep learning driven ultrasound tomography, Eksploatacja i Niezawodność – Maintenance and Reliability; 22 (2020), No 1, 138–147.
- [11] Gnaś, D., Adamkiewicz, P., Indoor localization system using UWB, Informatyka, Automatyka, Pomiary W Gospodarce I Ochronie Środowiska, 12 (2022), No. 1, 15-19.
- [12] Styła, M., Adamkiewicz, P., Optimisation of commercial building management processes using user behaviour analysis systems supported by computational intelligence and RTI, Informatyka, Automatyka, Pomiary W Gospodarce I Ochronie Środowiska, 12 (2022), No 1, 28-35.
- [13] Korzeniewska, E., Krawczyk, A., Mróz, J., Wysztyńska, E., Zawiślak, R., Applications of smart textiles in post-stroke rehabilitation, Sensors (Switzerland), 20 (2020), No. 8, 2370.
- [14] Sekulska-Nalewajko, J., Goćławski, J., Korzeniewska, E., A method for the assessment of textile pilling tendency using optical coherence tomography, Sensors (Switzerland), 20 (2020), No. 13, 1–19, 3687.
- [15] Colton, D., Kress, R., Integral Equation Methods in Scattering Theory, Springer, 1993.
- [16] Jabłoński P., Engineering Physics – Electromagnetism, Częstochowa University of Technology, 2009.
- [17] Kirkup S., The Boundary Element Method in Acoustics, Book in Journal of Computational Acoustics, January 2007.
- [18] Kirkup S., The Boundary Element Method in Acoustics: A Survey, Article in Applied Sciences, April 2019, DOI: 10.3390/app9081642
- [19] Lynott G.M., Efficient numerical evaluation of the scattering of acoustic and elastic waves by arrays of cylinders of arbitrary cross section, University of Manchester, School of Natural Sciences, Department of Mathematics, Thesis of Doctor of Philosophy, 2020.